Pleural innate response activator B cells protect against pneumonia via a GM-CSF-IgM axis

Pleural innate response activator B cells protect against pneumonia via a GM-CSF–IgM axis

Georg F. Weber,[1,2] Benjamin G. Chousterman,[1] Ingo Hilgendorf,[1] Clinton S. Robbins,[1] Igor Theurl,[1] Louisa M.S. Gerhardt,[1] Yoshiko Iwamoto,[1] Tam D. Quach,[3] Muhammad Ali,[1] John W. Chen,[1] Thomas L. Rothstein,[3] Matthias Nahrendorf,[1] Ralph Weissleder,[1,4] and Filip K. Swirski[1]

[1]Center for Systems Biology, Massachusetts General Hospital, Harvard Medical School, Boston, MA 02114
[2]Department of Visceral, Thoracic and Vascular Surgery, Medizinische Fakultät Carl Gustav Carus, Technische Universität Dresden, 01307 Dresden, Germany
[3]Center for Oncology and Cell Biology, The Feinstein Institute for Medical Research, Manhasset, NY 11030
[4]Department of Systems Biology, Harvard Medical School, Boston, MA 02115

Pneumonia is a major cause of mortality worldwide and a serious problem in critical care medicine, but the immunophysiological processes that confer either protection or morbidity are not completely understood. We show that in response to lung infection, B1a B cells migrate from the pleural space to the lung parenchyma to secrete polyreactive emergency immunoglobulin M (IgM). The process requires innate response activator (IRA) B cells, a transitional B1a-derived inflammatory subset which controls IgM production via autocrine granulocyte/macrophage colony-stimulating factor (GM-CSF) signaling. The strategic location of these cells, coupled with the capacity to produce GM-CSF–dependent IgM, ensures effective early frontline defense against bacteria invading the lungs. The study describes a previously unrecognized GM-CSF–IgM axis and positions IRA B cells as orchestrators of protective IgM immunity.

CORRESPONDENCE
F.K. Swirski:
fswirski@mgh.harvard.edu
OR
G.F. Weber:
georg.weber@uniklinikum-dresden.de

Abbreviations used: BAL, bronchoalveolar lavage fluid; CB, cord blood; CT, computed tomography; ICAPS, intercostal approach of the pleural space; i.n., intranasally; i.pls., into the pleural space; IRA, innate response activator; i.t., intratracheal.

Respiratory infections are an acute challenge in critical care medicine, typically affecting the very old, very young, and chronically ill. The Center for Disease Control and Prevention estimates that, in the United States, 1.7 million hospital-acquired respiratory infections claim 90,000 lives every year. This mortality rate is rising due to an increased number of immunosuppressed patients, exposure to drug-resistant organisms, and a growing elderly population (Mizgerd, 2008; Esperatti et al., 2010; Magret et al., 2011; Venkatachalam et al., 2011). There is, therefore, an urgent need to find novel therapeutic targets, and to do so requires deeper understanding of the disease's underlying pathophysiology.

Vertebrate animals rely on their diverse leukocyte populations to recognize and clear pathogens that breach mucosal barriers (Medzhitov, 2007). Infection of the lung mobilizes lymphocytes, granulocytes, and mononuclear phagocytes. Among the lymphocytes, the innate-like B1 B cells reside predominantly in serosal cavities. In response to infection, serosal B1 B cells relocate from either the pleural space or peritoneum and accumulate in either lung-draining lymph nodes or the spleen, respectively (Kawahara et al., 2003; Ha et al., 2006; Yang et al., 2007; Choi and Baumgarth, 2008; Moon et al., 2012). B1 cells are major producers of natural IgM antibodies that protect the host by opsonizing pathogens and promoting complement receptor–mediated phagocytosis (Boes et al., 1998; Baumgarth et al., 2000; Ansel et al., 2002; Fabrizio et al., 2007; Choi and Baumgarth, 2008; Racine and Winslow, 2009; Ehrenstein and Notley, 2010; Baumgarth, 2011; Litvack et al., 2011; Schwartz et al., 2012), but the mechanisms controlling B cell activation, as well as the consequences of relocating from serosal sites, are not fully known. We have recently shown in an abdominal sepsis model that peritoneal B1a B cells (a subset of B1 B cells) give rise to a population of B cells called innate response activator (IRA) B cells that produce the growth factor GM-CSF (Rauch et al., 2012). IRA B cells arise in the mouse by recognizing microbes via

The Rockefeller University Press $30.00
J. Exp. Med. 2014 Vol. 211 No. 6 1243-1256
www.jem.org/cgi/doi/10.1084/jem.20131471

The Journal of Experimental Medicine

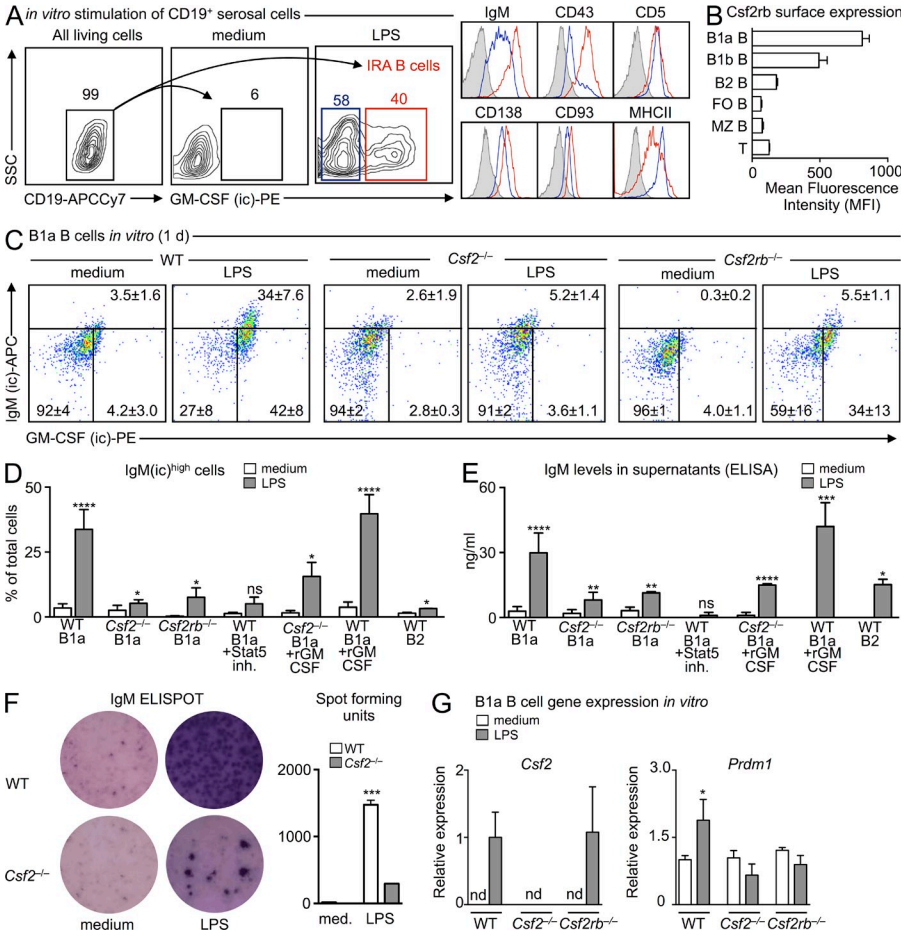

Figure 1. GM-CSF controls IgM production. (A) In vitro culture of CD19+ serosal B cells. Gating strategy and phenotyping of IRA B cells 2 d after culture in medium or with 10 µg/ml LPS. A representative contour plot of $n > 5$ is shown. (B) CD131 (Csf2rb) expression on selected cells from WT mice ($n = 4$). (C) In vitro culture of serosal B1a cells sorted from WT, *Csf2*$^{-/-}$, and *Csfrb*$^{-/-}$ mice. Data show intracellular IgM and GM-CSF in cells cultured in medium alone or after LPS (10 µg/ml) stimulation after 1 d of culture ($n = 3$–5). The gate for GM-CSF was set using an isotype control (IgG2a) and the gate for intracellular IgM represents the upper 99% limit of intracellular IgM staining at baseline. (D) In vitro culture of serosal B1a cells sorted from WT, *Csf2*$^{-/-}$, and *Csfrb*$^{-/-}$ mice, and B2 cells sorted from WT mice. Percentage of IgM(ic)^{high} cells cultured for 1 d in medium, after stimulation with 10 µg/ml LPS alone, or 10 µg/ml LPS + rGM-CSF, or with a Stat5 inhibitor ($n = 3$–8, mean ± SD). ns, not significant. (E) IgM ELISA of culture supernatants from the same groups as in D ($n = 3$–8, mean ± SD). ns, not significant. (F) IgM ELISPOT of cultured B1a cells. A representative ELISPOT of $n = 3$ is shown. (G) Quantitative RT-PCR analysis of *Csf2* and *Prdm1* expression in cultured serosal B1a cells from WT, *Csf2*$^{-/-}$, and *Csf2rb*$^{-/-}$ mice with and without LPS (10 µg/ml) stimulation for 1 d ($n = 3$). *Csf2* expression levels after LPS stimulation is shown relative to WT LPS as mean ± SD. *Prdm1* expression after LPS stimulation is shown relative to WT medium as mean ± SD (nd, not detected). *, $P < 0.05$; **, $P < 0.01$; ***, $P < 0.001$; ****, $P < 0.0001$.

TLR4 in the peritoneum and accumulate in large numbers in the splenic red pulp. The mechanisms by which B cell–derived GM-CSF protects against sepsis, however, are not known.

In this study, we show that in response to microbial airway infection, pleural B1a B cells relocate to the lung where they produce protective IgM. The process requires IRA B cells; animals with a B cell–restricted GM-CSF deficiency fail to secrete abundant IgM and consequently succumb to pneumonia. Mechanistically, autocrine GM-CSF activates B cells for IgM production via the common β chain receptor CD131. The study therefore identifies a GM-CSF-IgM activation axis that is critical in the response to infection and reveals the pleural space as a source of innate-like B cells that infiltrate the lung in response to bacterial lung infection.

RESULTS

GM-CSF controls IgM production

IgM production is a defining feature of innate-like B cells (Ehrenstein and Notley, 2010; Baumgarth, 2011; Cerutti et al., 2013). We have previously shown that IRA B cells are B1a-derived GM-CSF and IgM-producing cells (Rauch et al., 2012), whereas others have documented that GM-CSF can induce immunoglobulin secretion (Snapper et al., 1995). IgM and GM-CSF co-expression by the same cell prompted us to test for a direct link between the antibody and the growth factor. We sorted B1a B cells from serosal cavities (peritoneal and pleural), locations known to contain B1a B cells. After in vitro LPS stimulation, B1a B cells gave rise to GM-CSF–producing IRA B cells, defined as CD19^{+} IgM^{high} CD43^{+} CD5^{+} CD138^{+} CD93^{+} MHCII^{+} (Fig. 1 A). B1a B cells also expressed the common β chain high-affinity receptor for GM-CSF (Csf2rb, also known as CD131) at high levels (Fig. 1 B), which corresponded with transcriptional profiling data obtained by the Immunological Genome Project (ImmGen) and suggested that B cell–derived GM-CSF might be acting in an autocrine manner to produce IgM. To test this, we placed sorted B1a B cells from WT, *Csf2*$^{-/-}$ (i.e., GM-CSF–deficient), and *Csf2rb*$^{-/-}$ mice into culture and used flow cytometry to detect intracellular IgM reservoirs (Fig. 2, A and B). In response to LPS, WT but neither *Csf2*$^{-/-}$ nor *Csf2rb*$^{-/-}$ B1a B cells gave rise to a large population of IgM-producing cells (Fig. 1, C and D). GM-CSF was necessary but not sufficient to elicit robust IgM production because adding GM-CSF to WT cells in medium had no

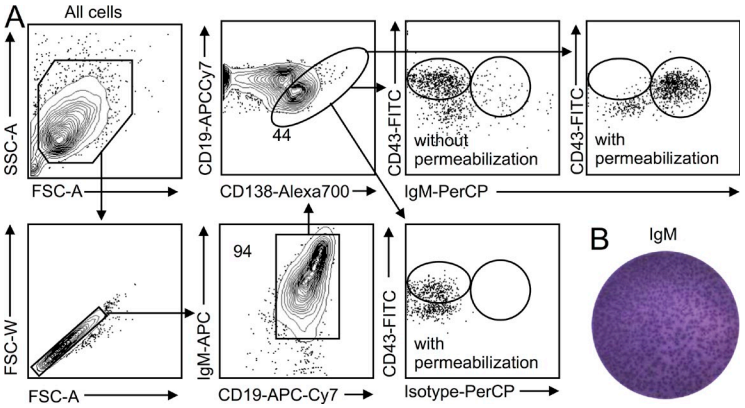

Figure 2. Intracellular staining of IgM. (A) Serosal B1a cells were sorted, placed in culture with LPS for 1 d, and stained for surface and intracellular IgM. Data show that the procedure can stain for intracellular IgM and that both surface and intracellular staining can be resolved. Surface IgM staining is followed by intracellular staining. A representative analysis of $n > 5$ is shown. (B) Validation of IgM production by ELISPOT on sorted B1a cavity cells 1 d after in vitro LPS stimulation. Shown is a representative analysis from $n > 5$.

effect. Adding recombinant (r) GM-CSF to *Csf2*$^{-/-}$ B1a cell cultures partially restored, whereas adding rGM-CSF to WT B1a cells augmented IgM production (Fig. 1 D). Although the rescue effect was partial in absolute values, the ∼10-fold increase of IgM by *Csf2*$^{-/-}$ cells after rGM-CSF was similar to that observed in WT cells. These data suggest that despite GM-CSF's absence during B1 cell development in *Csf2*$^{-/-}$ mice, which might affect the cells' ability to respond to LPS, a relatively robust response nevertheless occurs, providing evidence that GM-CSF stimulates IgM production. To illustrate the link between GM-CSF and IgM in WT cells, we focused on Stat5, which is crucial in the GM-CSF signaling pathway (Mui et al., 1995). Adding a Stat5 inhibitor to B1a cell cultures abrogated IgM production. B2 cells cultured with LPS likewise produced IgM, albeit at much lower levels. The intracellular IgM reservoirs correlated with secreted IgM, as measured by ELISA (Fig. 1 E) and ELISPOT (Fig. 1 F). RT-PCR confirmed that WT and *Csf2rb*$^{-/-}$ but not *Csf2*$^{-/-}$ cells produced GM-CSF in response to LPS (Fig. 1 G). When compared with *Csf2*$^{-/-}$ and *Csf2rb*$^{-/-}$ B1a B cells, stimulated WT B1a B cells expressed moderately higher levels of Prdm1 (Fig. 1 H), the gene which codes for Blimp-1, which is an essential transcription factor in plasma cell generation (Shapiro-Shelef et al., 2003; Savitsky and Calame, 2006; Fairfax et al., 2007; Nutt et al., 2007). In sum, the data show that B1a-derived IRA B cell secretion of GM-CSF promotes IgM production via CD131. This is a previously unrecognized GM-CSF-IgM axis that may be central to the early response to bacterial infection.

Protection against pneumonia requires pleural IRA B cells

The in vitro generation of IRA B cells from serosal B1a B cells led us to test whether IRA B cells can arise in the airways in vivo. We delivered LPS intranasally (i.n.) to WT mice and profiled the appearance of IRA B cells in various compartments 1 and 2 d later. Absolute IRA B cell numbers were highest in the lung and pleural space 2 d after LPS injection, with small numbers of IRA B cells accumulating in the bronchoalveolar lavage (BAL) and negligible numbers accumulating in both the lung-draining LN and blood at any point in time (Fig. 3, A and B). Expressing the increase of IRA B cells as a percentage of total B cells revealed dramatic increases in the pleural space, lung, and BAL (Fig. 3 C).

To determine whether IRA B cells are important in the host response to airway infection, we generated mixed chimeric mice with a B cell–restricted GM-CSF deficiency (Fig. 4). The procedure involved lethal irradiation of WT mice and reconstitution with a mixture of bone marrow cells from

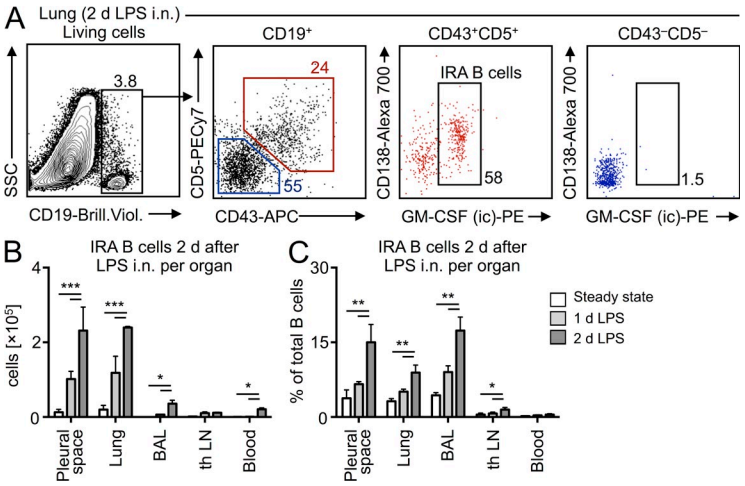

Figure 3. Identification of IRA B cells after airway challenge. (A) Identification of IRA B cells in the lung 2 d after LPS i.n. challenge. A representative dot plot of $n > 5$ is shown. (B) Enumeration of IRA B cells in different organs in steady-state and after LPS challenge ($n = 4$/group). (C) Enumeration as percentage increase ($n = 4$). Relevant data are presented as mean ± SD and tested by ANOVA; *, $P < 0.05$; **, $P < 0.01$; ***, $P < 0.001$.

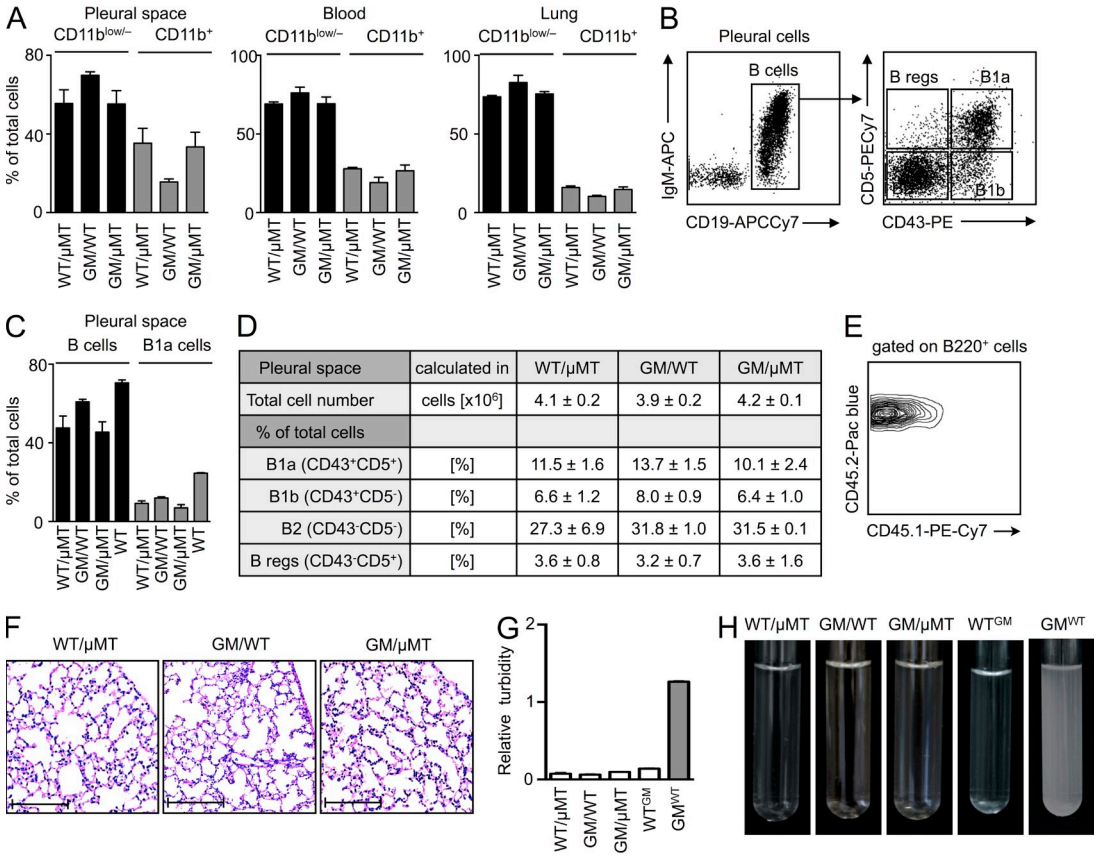

Pleural space	calculated in	WT/µMT	GM/WT	GM/µMT
Total cell number	cells [x10^6]	4.1 ± 0.2	3.9 ± 0.2	4.2 ± 0.1
% of total cells				
B1a (CD43$^+$CD5$^+$)	[%]	11.5 ± 1.6	13.7 ± 1.5	10.1 ± 2.4
B1b (CD43$^+$CD5$^-$)	[%]	6.6 ± 1.2	8.0 ± 0.9	6.4 ± 1.0
B2 (CD43$^-$CD5$^-$)	[%]	27.3 ± 6.9	31.8 ± 1.0	31.5 ± 0.1
B regs (CD43$^-$CD5$^+$)	[%]	3.6 ± 0.8	3.2 ± 0.7	3.6 ± 1.6

Figure 4. Generation of mixed chimeras. (A) Leukocyte reconstitution in WT/µMT, GM/WT, and GM/µMT mice in the pleural space, blood, and lung 10 wk after irradiation and bone marrow transfer. Data show the relative percentages of myeloid (CD11b$^+$) and nonmyeloid (CD11b$^-$) cells in the three compartments (n = 4, mean ± SD). (B) B cells in the pleural space of a WT mouse. Gating strategy for B1a (CD19$^+$IgM^{high}CD43$^+$CD5$^+$), B1b (CD19$^+$IgM^{high}CD43$^+$CD5$^-$), B2 (CD19$^+$IgM^{low}CD43$^-$CD5$^-$), and B reg (CD19$^+$IgM$^+$CD43$^-$CD5$^+$) B cells is shown. (C) Relative proportions of total B cells and B1a B cells in the pleural space of WT/µMT, GM/WT, and GM/µMT chimeric mice and non-irradiated WT mice in the steady state. The chimeric mice were analyzed 8 wk after bone marrow transfer (n = 3–5, mean ± SD). (D) Enumeration of the various subsets in the three chimeras (n = 3–5, mean ± SD). (E) CD45.2 expression on blood leukocytes in CD45.1$^+$ mice that had been lethally irradiated and reconstituted with CD45.2$^+$ bone marrow cells 10 wk earlier. The plot is representative from that of the three chimeras. (F) Lung H&E in the three sets of chimeric mice 10 wk after bone marrow reconstitution (bars, 200 µm). (G) Turbidity analysis of BAL at 600 nm from WT/µMT, GM/µMT, WT^{GM} (lethal irradiation of WT mouse and 100% reconstitution with *Csf2*$^{-/-}$ BM), and GM^{WT} (lethal irradiation of *Csf2*$^{-/-}$ mouse and 100% reconstitution with WT BM) chimera (n = 3; mean ± SD). (H) BAL of WT/µMT, GM/WT, GM/µMT, WT^{GM}, and GM^{WT} chimeric mice.

µMT and GM-CSF–deficient mice. Accordingly, the µMT bone marrow gave rise to GM-CSF–sufficient leukocytes, but not B cells, whereas the GM-CSF–deficient bone marrow gave rise to GM-CSF–deficient leukocytes, including B cells. After 10 wk of reconstitution, all B cells (which necessarily derived from GM-CSF–deficient mice) lacked the capacity to produce GM-CSF in the mixed chimeras (GM/µMT). The remaining leukocytes were a mixture of WT and GM-CSF–deficient cells, whereas radiation-resistant and tissue-resident nonhematopoietic cells were GM-CSF–sufficient. We also generated two types of controls: WT mice reconstituted with a mixture of WT and µMT bone marrow cells (WT/µMT), which controlled for the µMT contribution, and WT mice reconstituted with a mixture of GM-CSF–deficient and WT bone marrow cells (GM/WT), which controlled for the contribution of any GM-CSF–deficient non–B cells in the GM/µMT group. The leukocyte profiles in the pleural space, blood, and lung in the steady-state were most similar between the GM/µMT and WT/µMT chimeras (Fig. 4 A), but all three chimeras developed various B cell subsets (Baumgarth, 2011), including B1a B cells, as expected (Düber et al., 2009; Esplin et al., 2009; Holodick et al., 2009). Even though reconstitution was sub-optimal compared with non-irradiated WT mice (Fig. 4, B–D), the chimeras' leukocytes were of donor origin (Fig. 4 E), and the mice had normal lung histology (Fig. 4 F) without evidence of alveolar proteinosis (Fig. 4, G and H). Complete GM-CSF deficiency leads to the development of spontaneous alveolar proteinosis (Dranoff et al., 1994; Stanley et al., 1994). Previous data have shown (Huffman et al., 1996), and our data confirm, that pulmonary epithelial (i.e., nonhematopoietic) GM-CSF–producing cells prevent proteinosis by stimulating alveolar macrophages to clear surfactant; B cells are dispensable in this context.

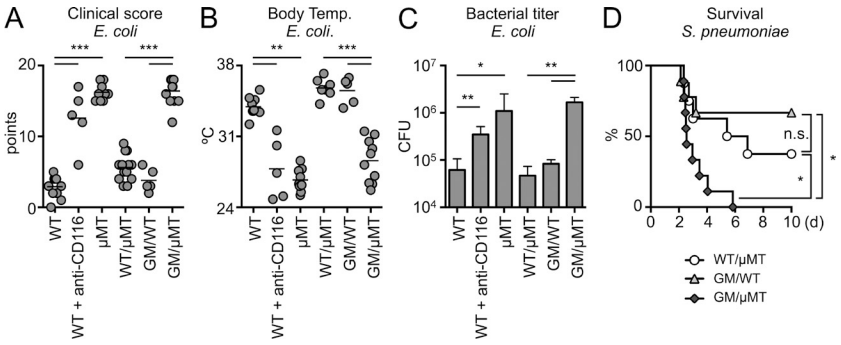

Figure 5. IRA B cells protect against pneumonia. (A) Clinical score of WT, WT receiving anti-CD116, μMT, WT/μMT, GM/WT, and GM/μMT mice 9 h after infection with *E. coli* (n = 5–10 mice). (B) Body temperature of the groups above. (C) Bacterial titer in BAL after *E. coli* infection of WT, WT receiving anti-CD116, μMT, WT/μMT, GM/WT, and GM/μMT mice (n = 5–10 mice). (D) Kaplan-Meier survival curves after *S. pneumoniae* i.t. infection for WT/μMT, GM/WT, and GM/μMT mice (n = 8–10). Relevant data are presented as mean ± SD and tested by ANOVA; *, $P < 0.05$; **, $P < 0.01$; ***, $P < 0.001$.

After reconstitution, we infected GM/μMT, WT/μMT, and GM/WT mice with *Escherichia coli*. Although *E. coli* are not the predominant pneumonia-causing pathogen, they are Gram-negative, LPS-bearing bacteria and are responsible for a significant proportion of hospital-acquired pneumonias (Williams et al., 2002; Klevens et al., 2007; Scott et al., 2008; Esperatti et al., 2010; Jones, 2010; Magret et al., 2011; Venkatachalam et al., 2011). We monitored infected mice for morbidity and bacterial titer. As additional controls, we infected WT, B cell–deficient μMT mice (i.e., nonirradiated, nonchimeric), and WT mice that received anti-CD116 intrapleurally (i.e., anti–GM-CSFRα, the subunit of the GM-CSF receptor which is specific to GM-CSF; the antibody has been reported to be neutralizing). Three groups of mice—μMT, WT receiving anti-CD116, and chimeric GM/μMT (i.e., IRA KO)—became very morbid (Fig. 5 A), hypothermic (Fig. 5 B), and had increased bacterial counts in the BAL (Fig. 5 C). In contrast, WT mice and the two chimeric controls were more resistant to infection. The data show that B cell–derived GM-CSF is important and beneficial to the early response to airway infection. The similarity between μMT and GM/μMT mice in failing to protect against infection illustrates that GM-CSF production by B cells is an essential component of the overall B cell response at this early time point. Blocking CD116, GM-CSF's specific receptor subunit, confirmed that GM-CSF signaling is important in WT mice in vivo. We also wondered whether the key finding that IRA B cells are protective was specific to *E. coli* or might also apply to other bacterial pathogens. GM/μMT mice infected with *Streptococcus pneumoniae*, a major cause of disease in humans worldwide and the primary pathogen responsible for pneumonia (Mizgerd, 2008), died earlier and in larger numbers than controls (Fig. 5 D). These data underscore the importance of IRA B cells in pneumonia, thereby prompting us to delve further into these protective processes.

Impaired IgM production in the absence of IRA B cells

Having observed that B cell–derived GM-CSF protected against pneumonia, we next examined the mixed chimeras' cellular and humoral response, particularly whether the absence of B cell–derived GM-CSF associates with impaired IgM production in vivo. In the steady-state, IgM was readily detectable, and its similar concentrations in GM/μMT and WT/μMT mice indicated that IRA B cells are dispensable to steady-state IgM production. After infection, control but not GM/μMT mice showed augmented IgM in the pleural space, lung, and serum, indicating impaired emergency IgM production in mice lacking IRA B cells (Fig. 6 A). Immunofluorescence microscopy showed lung B cells in GM/μMT mice to be weakly positive for IgM compared with controls (Fig. 6 B). The data suggest that B cell–derived GM-CSF is required for IgM production in vivo in response to lung infection.

Given GM-CSF's reported role in emergency hematopoiesis (Zhan et al., 1998), we also tested whether the absence of B cell–derived GM-CSF impaired the generation of monocytosis and granulopoiesis. Surprisingly, the GM/μMT chimeras generated more, not fewer, myeloid cells. Compared with WT/μMT controls, GM/μMT mice had higher numbers of neutrophils in the lungs, blood, and bronchoalveolar lavage (BAL) fluid (Fig. 6, C and D). Interestingly, neutrophils in GM/μMT mice phagocytosed bacteria poorly (Fig. 6 E), possibly reflecting insufficiency of IgM, an isotype known to facilitate complement receptor–mediated phagocytosis (Baumgarth, 2011; Schwartz et al., 2012). Finally, GM/μMT mice expressed higher levels of the inflammatory mediators IL-1α, IL-6, TNF, and CXCL1 in the BAL (Fig. 6 F). We did not detect IL-10 in the groups, which argues against a B regulatory phenotype in this model. Thus, impaired IgM production, rather than impaired myelopoiesis, appeared to contribute to infection susceptibility in animals lacking B cell–derived GM-CSF.

Pleural B1a B cells migrate to the lung parenchyma

Coelomate animals contain peritoneal, pleural, and pericardial cavities that shield and support internal organs. The pleural cavity is the space between the outer parietal pleura attached to the chest wall and the inner visceral pleura that covers the lungs. Its primary purpose may be to aid lung function, as the pleural fluid allows the membranes to slide effortlessly during ventilation, but the space also contains immune cells such as macrophages and B cells. Such leukocyte location could be strategic; pleural cells may function as either sentinels against barrier-breaching or reservoirs for lung infiltration. Our observations that serosal B1a B cells can give rise to IRA B cells in vitro (Fig. 1 A); that IRA B cells arise in the pleural space/lung during airway infection (Fig. 3); and that B cell–derived GM-CSF controls IgM production in the airways

(Fig. 6, A–C) prompted the hypothesis that the pleural space sources lung-infiltrating IgM-producing B cells in response to bacterial airway infection. To test this, we developed the intercostal approach of the pleural space (ICAPS) method (Fig. 7 A), in which a catheter is intercostally inserted into the organism's thorax at a low angle to bypass the diaphragm and reduce the risk of puncturing the lung. When the catheter is removed, the intercostal muscles seal the puncture canal and prevent a pneumothorax. We confirmed the validity of this procedure by injecting a CT imaging contrast agent into the pleural space (Fig. 7 B) and transferring GFP$^+$ leukocytes for in vivo fate mapping (Fig. 7 C).

To track leukocyte migration, we transferred total pleural and peritoneal GFP$^+$ cells to either the pleural or peritoneal space of mice receiving LPS. 2 d after transfer, we enumerated GFP$^+$ cells that had accumulated in various organs. Cells transferred to the pleural space accumulated in the lung preferentially and were enriched for B cells (Fig. 7, D and E). In contrast, only a small number of GFP$^+$ cells accumulated in the lung from the peritoneum, and only a small number of cells accumulated in the spleen from either source (Fig. 7 E). To focus on pleural B1a B cells specifically, we adoptively transferred sorted pleural GFP$^+$ B1a B cells to the pleural space. After 2 d of LPS challenge, a substantial fraction (~26%) of all B1a cells in the lung were GFP$^+$ (Fig. 7 F), and the cells were readily visible by fluorescence microscopy (Fig. 7 G). The pleural space, but not the blood, still contained many GFP$^+$ B1a B cells at this time point (Fig. 7 F), which suggested that pleural B1a cells relocated directly from the pleural space to the lungs. Indeed, pleural cells were readily observed in regions close to the mesothelial layer, the single-cell barrier known to express adhesion molecules—such as VCAM-1 (Jonjić et al., 1992)—that separates lung tissue from the pleural space.

Pleural B1a B cells produce protective IgM in the lungs

The leukocyte profile and the differences between the two delivery routes suggested that the pleural space was the preferential

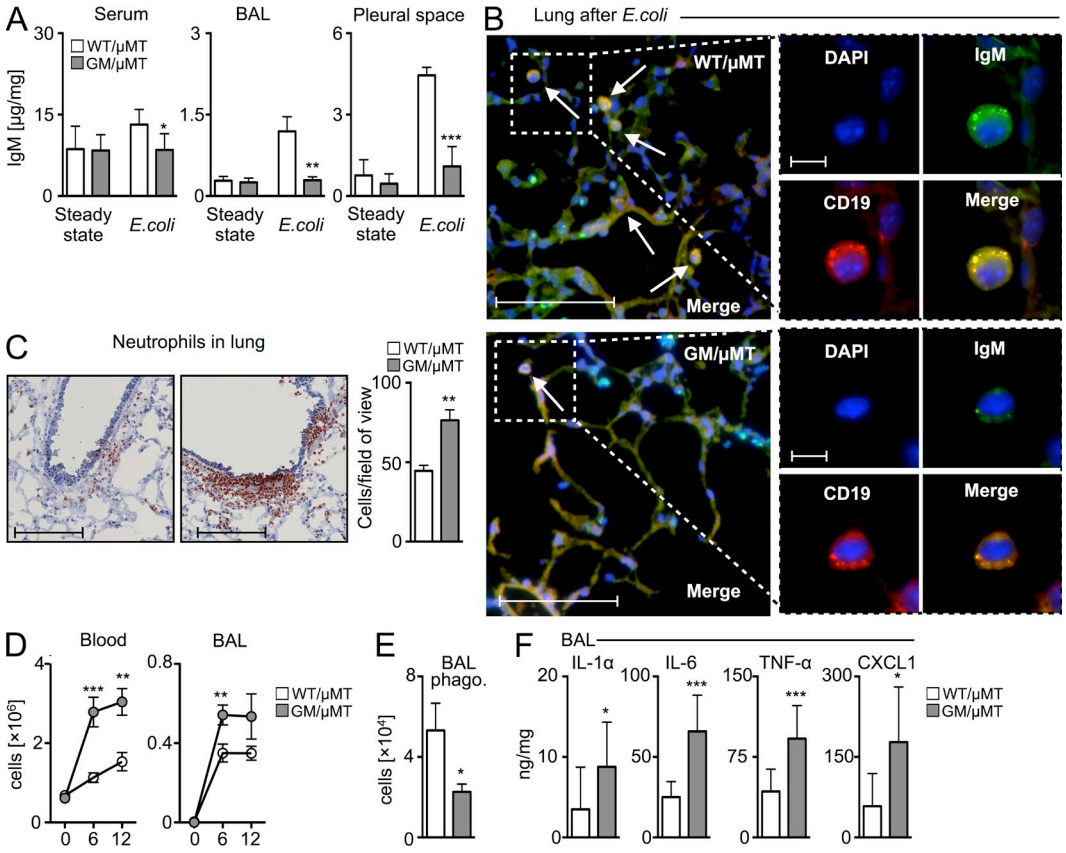

Figure 6. Enhanced inflammation but attenuated IgM after *E. coli* airway infection in the absence of IRA B cells. (A) IgM levels detected by ELISA in serum, BAL, and pleural space 9 h after *E. coli* infection (n = 6–10 mice). (B) Lung histology after *E. coli* infection. DAPI: blue; CD19: red; IgM: green; merge: yellow. Representative pictographs of n = 6–10 animals/group are shown (bars: overview, 100 µm; inset, 10 µm). Arrows indicate IgM$^+$CD19$^+$ cells. (C) Analysis of WT/µMT and GM/µMT mice after i.t. *E. coli* infection. Immunohistochemical staining for neutrophils in lung tissue and enumeration of neutrophils measured by counts of neutrophils per field of view. A representative slide of n = 6–10 is shown (bars, 400 µm). (D) Enumeration of neutrophils in blood and BAL (n = 6–10). (E) Analysis of the phagocytic capacity of neutrophils from the BAL of WT/µMT and GM/µMT mice. Shown are total cell numbers with phagocytosed Pkh26$^+$ bacteria (n = 4). (F) Analysis of BAL levels for IL-1α, IL-6, TNF, and CXCL1 (n = 5–15 mice). Relevant data are presented as mean ± SD; *, P < 0.05; **, P < 0.01; ***, P < 0.001.

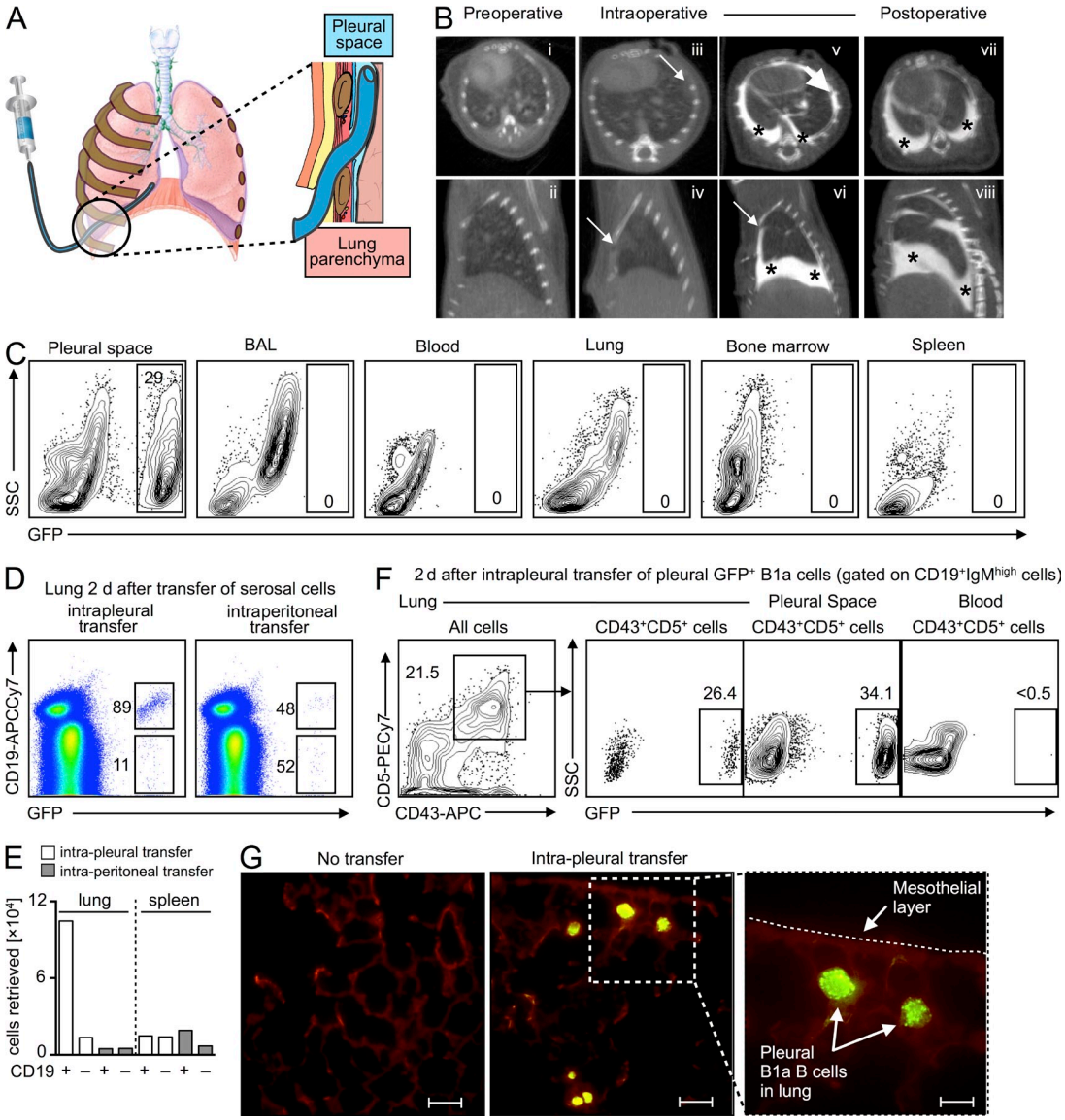

Figure 7. The pleural space is a reservoir of lung-infiltrating B1a B cells. (A) Cartoon depicting the ICAPS model. After skin incision, a small catheter can be navigated through the intercostal space and placed in the pleural space. (B) Preoperative: (i and ii) CT scans before insertion of the catheter. Intraoperative: (iii and iv) CT scans immediately after insertion of the catheter. (v and vi) CT scans after injection of 300 µl Iopamidol iodine CT contrast agent. Postoperative: (vii and viii) CT scans 10 min after the catheter was removed. There were no signs of injection into lung parenchyma, pneumothorax, or leakage (top row of CT scans: axial view; bottom rows of CT scans: sagittal view; arrows denote the tip of the catheter; stars donate the injected Iopamidol iodine CT contrast agent). (C) Intrapleural (i.e., by ICAPS) transfer of GFP+ serosal cells. Cells were transferred into WT mice which were sacrificed 10 min after transfer. Data show transferred cells in the pleural space, BAL, blood, lung, bone marrow, and spleen. (D) Unsorted GFP+ serosal cells were adoptively transferred to the pleural or peritoneal spaces of WT mice that received pulmonary LPS challenge. Data show profile of lung accumulation in recipients 2 d after transfer. A representative experiment of $n = 5$ is shown. (E) Enumeration of CD19+ and CD19− cells accumulating in the lung and spleen after intrapleural or intraperitoneal transfer of unsorted GFP+ serosal cells. A representative enumeration of $n = 5$ is shown. (F) Intrapleural adoptive transfer of serosal B1a GFP+ cells. Data show frequency of adoptively transferred (GFP+) cells in the lung, pleural space, and blood 2 d after pulmonary LPS challenge. A representative dot plot from $n = 4$ is shown. (G) Fluorescence microscopy of lung tissue 2 d after intrapleural adoptive transfer of sorted GFP+ serosal B1a cells (bars: overview, 20 µm; inset, 10 µm).

source of lung-accumulating serosal B cells. B1a B cells retrieved from the lung contained large reservoirs of IgM (Fig. 8, A and B), which they secreted locally, as measured by ELISPOT assays performed on GFP+ cells that had relocated from the pleural space to lung tissue (Fig. 8 C). To determine the importance of pleural B cells to the host response, we profiled mortality in WT and µMT (i.e., B cell–deficient) mice infected with a high dose of *E. coli*. After 48 h, ∼40% of WT mice died but ∼60% completely recovered. In contrast, ∼80% of B cell–deficient µMT mice died within 12 h (Fig. 8 D).

Additionally, we used ICAPS to transfer pleural B cells from WT mice to the pleural spaces of μMT mice. The μMT pleural B cell recipients, which now contained B cells but only in the pleural space, were then infected with *E. coli*. Remarkably, this B cell supplementation completely reversed the severe mortality otherwise observed in μMT mice (Fig. 8 D). For controls, we transferred pleural B cells from *Csf2*$^{-/-}$ mice to the pleural spaces of μMT mice and B cells sorted from the blood of WT mice to the blood (by i.v.) of μMT mice. Neither approach rescued the μMT mice, indicating that GM-CSF produced by pleural B cells was required for protection. The data show that pleural B cells defend against pneumonia.

IgM is one of the first antibody isotypes secreted during infection. IgM recognizes multiple epitopes with low affinity and is therefore polyreactive and innate-like, but its pentameric structure increases avidity and allows for potent opsonizing and complement-fixing functions. To determine whether IgM recognized bacteria in our model, we infected μMT mice and μMT mice that received pleural B cells into the pleural space (Fig. 8 E) with Pkh26-labeled *E. coli*. 6 h later, the BAL fluid contained labeled bacteria in both groups, but only bacteria in μMT animals receiving pleural B cells were opsonized with IgM (Fig. 8 E). Newly produced IgM (i.e., IgM retrieved from the BAL 6 h after LPS intratracheal [i.t.] delivery) recognized gram-positive *Staphylococcus aureus* and gram-negative *Pseudomonas aeruginosa*, indicating polyreactivity (Fig. 8 F). Moreover, IgM titers were increased in the BAL and pleural space of μMT mice receiving WT pleural B cells but not *Csf2*$^{-/-}$ pleural B cells (Fig. 8 G). These data indicate that in response to airway infection, pleural B cells relocate to the lung and produce opsonizing, polyreactive, GM-CSF–dependent IgM.

Secreted IgM is necessary for protection against pneumonia

At this point, the data can be summarized as follows: in response to pulmonary infection, IRA B cells arise in the pleural space and lung; in the absence of IRA B cells (absence of B cell–derived GM-CSF), mice fail to produce IgM and succumb to pneumonia; and pulmonary infection mobilizes pleural B1a B cells, which relocate to the lung and produce IgM. To further validate these findings, we wished to test the importance of pleural B cell–derived GM-CSF and secreted IgM in our model. We pursued a rescue strategy involving the adoptive transfer of different cell populations to the pleural spaces of GM/μMT mice. We transferred *Csf2*$^{-/-}$ pleural B cells, WT pleural non–B cells, pleural B cells from secretory IgM-deficient (sIgM$^{-/-}$) mice, and WT pleural B cells (Fig. 9 A). Comparing the adoptive transfer of WT pleural B cells with *Csf2*$^{-/-}$ pleural B cells and WT pleural non–B cells allowed us to determine the importance of B cell–derived GM-CSF, whereas sIgM$^{-/-}$ mice demonstrated the importance of secreted IgM. Mice that received WT pleural B cells into the

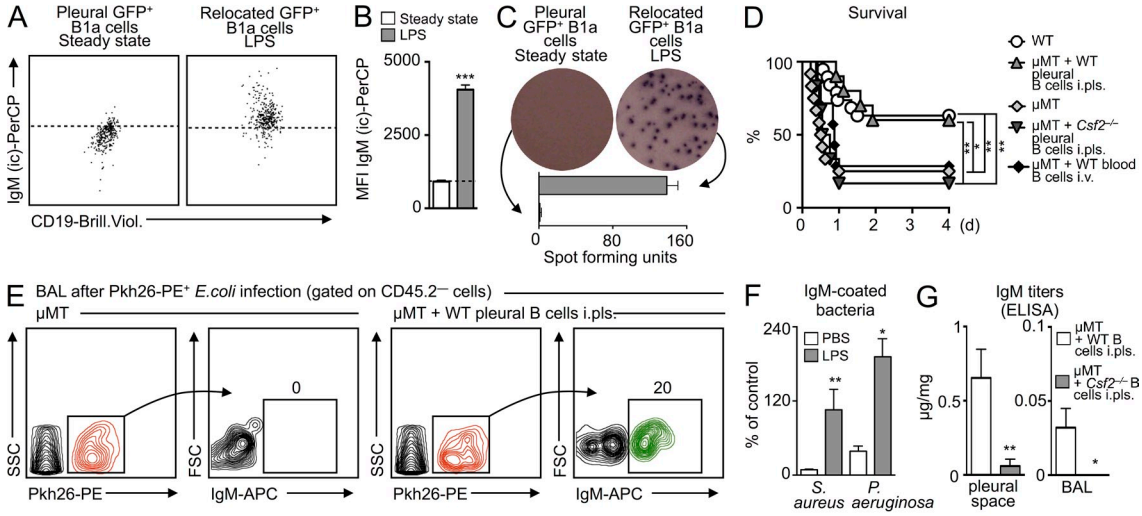

Figure 8. Pleural B1a B cells accumulating in the lung produce opsonizing IgM that is sufficient to confer survival. (A) Intracellular IgM (IgM (ic)) reservoirs in steady-state pleural GFP+ B1a cells (left dot plot) and in GFP+ B1a cells that had infiltrated LPS-challenged lungs after intrapleural transfer (right dot plot). The dotted line represents the upper 99% limit of intracellular IgM staining in steady-state cells. Representative analysis from $n = 4$ is shown. (B) Mean fluorescence intensity (MFI) of IgM (ic) from A ($n = 4$). (C) IgM ELISPOT analysis of cells as in A. Representative analysis from $n = 2$ experiments is shown. (D) Kaplan-Meier survival curves in response to *E. coli* infection in WT mice; μMT mice; and μMT mice that received WT pleural B cells in the pleural space, *Csf2*$^{-/-}$ pleural cells in the pleural space, and WT blood cells into the blood at the time of infection ($n = 10$ mice). (E) Opsonization of bacteria with IgM. Data show Pkh26-labeled *E. coli* retrieved from the BAL of either μMT mice or μMT mice spiked with pleural WT B cells in the pleural space. Bacteria (i.t.) and cell transfer (i.pls.) were conducted 6 h before BAL. An antibody against IgM shows opsonization of labeled bacteria. A representative analysis of $n = 3$ is shown. (F) IgM is polyclonal. WT mice received PBS or LPS. 6 h later, BAL was collected, and capacity of IgM to bind to *S. aureus* and *P. aeruginosa* was measured. Data show binding relative to a commercially available polyclonal IgM ($n = 3$). (G) IgM ELISA of pleural fluid and BAL after *E. coli* infection. μMT mice received WT or *Csf2*$^{-/-}$ pleural B1a cells into the pleural space at the time of infection ($n = 3$). Relevant data are presented as mean ± SD; *, $P < 0.05$; **, $P < 0.01$; ***, $P < 0.001$.

pleural space were healthier, as judged by their clinical scores, body temperatures, and bacterial titers (Fig. 9 B). Moreover, mice that received WT pleural B cells had increased titers of IgM (Fig. 9 B). That none of the other three strategies protected the animals indicated that B cell–derived GM-CSF is essential. To determine whether polyclonal IgM could indeed rescue IRA B cell–deficient, GM/μMT chimeras, we injected polyclonal IgM i.t. into GM/μMT mice infected with a high dose of *E. coli*. Compared with controls receiving PBS, poly-IgM recipients were protected (Fig. 9 C).

Previously, we demonstrated that the human spleen contains a population of GM-CSF–producing IRA B-like cells (Rauch et al., 2012). To determine whether humans also contain, or can develop, IRA B-like cells in the pleural space, we obtained human pleural fluid by thoracentesis, and cultured B cells in either medium or a classical human B cell stimulation cocktail containing anti-Ig and IL-2. After 2 d of culture, human pleural $CD19^+$ $CD20^+$ IgM^+ B cells produced GM-CSF (Fig. 10, A–C). The GM-CSF producers clustered in a single rather than bimodal distribution, suggesting indiscriminate activation in this in vitro setting. To reveal whether the appearance of IRA B-like cells was unique to the pleural space, we also cultured B cells from cord and peripheral blood. In the cord blood, which contains predominantly naive and transitional cells, a large GM-CSF–producing population likewise arose (Fig. 10 C). In contrast, culturing peripheral blood B cell did not stimulate GM-CSF production (Fig. 10 C), a result which supports the concept that IRA B cells arise in specific locations. Adding nontoxic doses of anti–GM-CSF, anti-CD116, or a STAT5 inhibitor to the culture containing pleural cells prevented the appearance of IRA B-like cells, further indicating an important role of the GM-CSF pathway (Fig. 10 D). Although further work is required to elucidate the similarities and differences between murine and human IRA B cells, these data nevertheless illustrate our current findings' potential translatability. In sum, the production of GM-CSF by IRA B cells orchestrates the generation of protective IgM, which is critical in the early defense to infection (Fig. 10 E).

DISCUSSION

The innate immune mechanism described here clears bacteria and protects against pneumonia. We show that in response to infection, pleural B cells relocate to the lung and produce abundant natural IgM, which is known to protect against infection (Boes et al., 1998; Baumgarth et al., 2000; Fabrizio et al., 2007; Choi and Baumgarth, 2008; Litvack et al., 2011; Schwartz et al., 2012). B cell–derived GM-CSF is the autocrine instructor required for emergency IgM production. Recently identified IRA B cells, which differentiate from B1a B cells in the mouse via direct TLR-dependent pathogen recognition, are key to this process and therefore to early innate immune defense.

GM-CSF was identified in the 1960s as a colony stimulator of granulocytes and mononuclear cells, though not erythrocytes (Bradley and Metcalf, 1966). GM-CSF–deficient mice, which were independently generated by two groups in 1994 (Dranoff et al., 1994; Stanley et al., 1994), show no striking perturbations of hematopoiesis in the steady state but develop alveolar proteinosis. This condition's human counterpart is characterized by elevated anti–GM-CSF autoantibodies (Carey and Trapnell, 2010). In the mouse, GM-CSF is produced by pulmonary epithelial cells (Huffman et al., 1996), T cells, and macrophages (Hamilton, 2008; Hamilton and Achuthan, 2013). The growth factor promotes the maturation, survival,

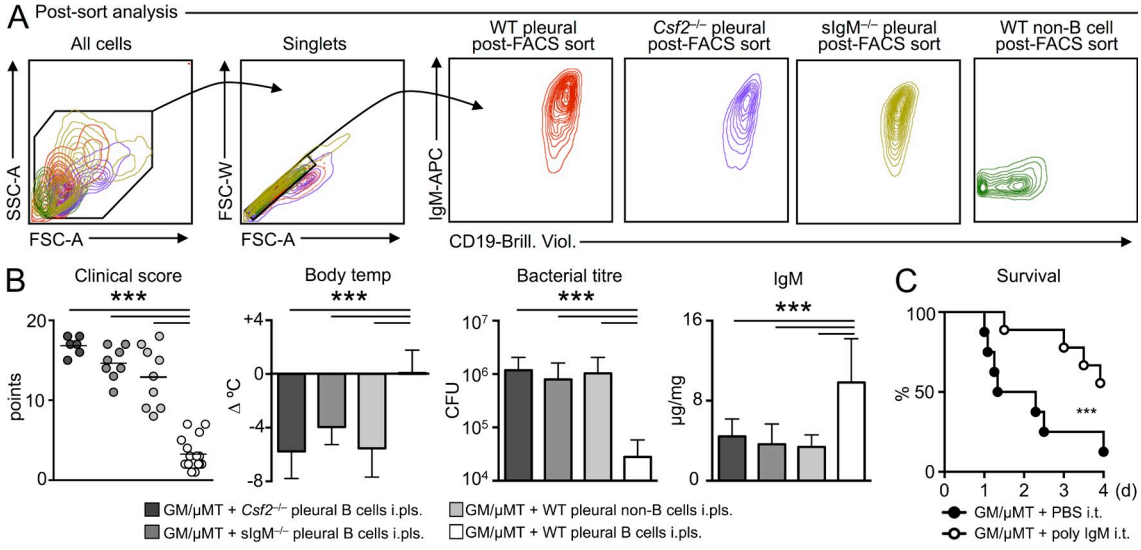

Figure 9. IRA B cells and secreted IgM are required for protection against pneumonia. (A) Postsort analysis of sorted WT, $sIgM^{-/-}$, $Csf2^{-/-}$ serosal B cells, or WT serosal non–B cells. Representative plots are shown of $n > 10$. (B) GM/μMT (i.e., IRA B cell KO) mice received intrapleural transfer of WT, $sIgM^{-/-}$, $Csf2^{-/-}$ serosal B cells, and WT non–B cells ($n = 6$–15 mice). 6 h later, mice were infected i.t. with *E. coli*. 9 h later, clinical score, body temperature, bacterial titer in the BAL, and IgM in serum were measured. Data are presented as mean ± SD and tested by ANOVA. (C) Kaplan-Meier Survival Curve of GM/μMT mice infected with *E. coli* receiving either PBS or polyclonal IgM i.t. ($n = 10$). Relevant data are presented as mean ± SD; ***, $P < 0.001$.

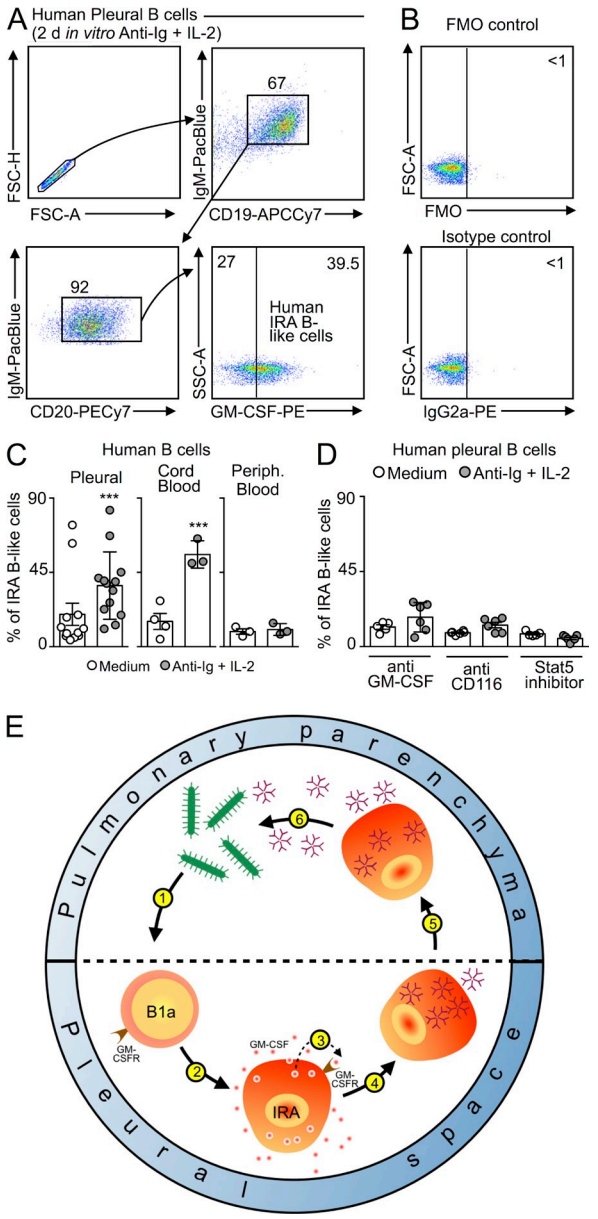

Figure 10. IRA B cells in humans. (A) Human pleural B cells were placed in vitro for 2 d and stimulated with anti-Ig and IL-2. Data show the appearance of GM-CSF–producing, IRA-like B cells. (B) Fluorescence-minus-one (FMO) and isotype controls of stimulated human B cells. (C) Total B cells were collected from human pleural space, cord blood, and peripheral blood and cultured for 2 d either in medium or with anti-Ig and IL-2 stimulation. Data show quantity of IRA-like B cells appearing in each condition. (D) Total B cells from the pleural space were cultured as in C, and with anti–GM-CSF, anti-CD116, or a Stat5 inhibitor. Data show quantity of IRA-like B cells appearing in each condition (n = 4–15). Relevant data are presented as mean ± SD. ***, $P < 0.001$. (E) Model for the function of IRA B cells in mouse pneumonia. During airway infection pleural space B1a cells recognize bacteria or its components (1). This leads to the generation (2) of IRA B cells which produce GM-CSF and express the GM-CSF receptor. GM-CSF acts on its receptor in an autocrine (3) manner. The signaling orchestrates generation of IgM-producing cells (4) which relocate to the lung (5). IgM derived from pleural space B cells is essential to the control of bacteremia (6).

and proliferation of its target cells; it controls nonlymphoid tissue dendritic cell homeostasis (Greter et al., 2012), emergency granulopoiesis (Kimura et al., 2009), iNKT cell differentiation (Bezbradica et al., 2006), sensitization to allergen (Stämpfli et al., 1998), and other effects related to immune activation (Hege et al., 2006; Timmerman et al., 2009; Le et al., 2010). In vitro, GM-CSF remains a standard for differentiating bone marrow progenitors to dendritic cells.

The early appearance of a unique GM-CSF–producing B cell in sepsis suggests a leukocyte communication hierarchy in which IRA B cells educate their client myeloid cells. A major finding of this study is therefore unexpected: IRA B cells produce GM-CSF for themselves. This autocrine function is all the more surprising considering its outcome, which is IgM production. At the signaling level, this may involve Blimp-1, a transcriptional repressor required for the formation of immunoglobulin-secreting B1-derived plasma cells (Shapiro-Shelef et al., 2003; Savitsky and Calame, 2006; Fairfax et al., 2007; Nutt et al., 2007) and Stat5, a transcription factor downstream of GM-CSF signaling (Mui et al., 1995; Kimura et al., 2009) which has been recently shown to amplify Blimp-1 in T cells (Nurieva et al., 2012). Future studies will need to elucidate the precise sequence of events that link GM-CSF signaling to IgM production. In addition to investigating how signals downstream of GM-CSF and LPS integrate, activate Stat5 and Blimp-1, and cooperate to produce IgM, additional questions remain as to whether and how GM-CSF contributes to the generation of mature B1 cells. Because pleural B cells can also accumulate in the lung-draining lymph nodes (Choi and Baumgarth, 2008), future work must determine whether IRA B cell–derived GM-CSF elicits other responses, such as generating or activating dendritic cells.

Many cytokines have an endocrine function. IL-1β, IL-6, and TNF, for example, travel in the bloodstream and affect tissues at distance from injury or infection. Evidence suggests that GM-CSF's activity is more spatially restricted. Serum levels of GM-CSF tend to be low in steady state and inflammation because of receptor and autoantibody-mediated clearance (Metcalf et al., 1999). GM-CSF's pleiotropy relies on a binary, concentration-dependent switch (Guthridge et al., 2006). In this study, we show that B cell–derived GM-CSF is necessary for protective IgM responses but dispensable to surfactant clearance by alveolar macrophages. The cellular source and location of GM-CSF, our data indicate, is important and may be particularly relevant during clinical intervention. Indeed, on the basis of GM-CSF's capacity to augment HLA-DR and potentially arm the host for effective immunity, clinical trials have explored using recombinant GM-CSF for sepsis treatment (LaRosa and Opal, 2012). A few studies showed an all-survival benefit, but a meta-analysis found no consensus among the trials, and thus no evidence to support routine GM-CSF use (Bo et al., 2011). In all trials, however, GM-CSF was delivered either intravenously or subcutaneously. Future studies will need to determine whether locally administering GM-CSF to strategic locations, such as the

pleural space, can overcome host clearance mechanisms and engender a durable clinical benefit.

The adaptive arm of the immune system requires lymphoid tissues in which leukocytes interact, proliferate, and, over time, generate antigen specificity and memory. For innate immunity to be effective, it must respond to a different challenge: it has to act quickly. The pleural space's proximity to the lung gives pleural leukocytes an advantage in meeting this challenge. The observation that pleural space B cells control the early response to infection is significant because it broadens our understanding of the immune system's spatio-cellular dynamics. Additionally, the mechanistic insight that a particular B cell controls this event via a previously unrecognized GM-CSF-IgM axis might have important biological and therapeutic implications for the treatment of infectious diseases.

MATERIALS AND METHODS

Animals

C57BL/6J (WT), B6.SJL-PtprcaPepcb/BoyJ (CD45.1$^+$), C57BL/6-Tg(UBC-GFP)30Scha/J (GFP$^+$), and B10.129S2(B6)-Ighmtm1Cgn/J (μMT) female mice (The Jackson Laboratory) were used in this study. GM-CSF–deficient mice (*Csf2*$^{-/-}$) were a gift from R. Seeley (University of Cincinnati, Cincinnati, OH). Secretory IgM-deficient mice (sIgM$^{-/-}$) were a gift from K. Alugupalli (Thomas Jefferson University, Philadelphia, PA). GM-CSF receptor-deficient mice (*Csf2rb*$^{-/-}$) were a gift from J. Whitsett (Cincinnati Children's Hospital Medical Center, Cincinnati, OH). All mice were 8–20 wk of age at the time of sacrifice. All protocols were approved by the Animal Review Committee at Massachusetts General Hospital.

Animal models and in vivo interventions

For the adoptive transfer of cells i.v., i.p., or into the pleural space (i.pls.), mice were anesthetized with isoflurane.

Intrapleural injection using the ICAPS model. After fixation of the mice with tape, a right anterolateral thoracic incision was performed over 2–3 cm, followed by careful sharp dissection of the attached muscles from the thoracic wall. A polyethylene catheter (Intramedic, I.D. 0.28 mm; BD) was then tangentially inserted into the pleural space without harming the lung parenchyma. Cells, contrast agent, or PBS was injected. After removing the catheter, we controlled for pneumothorax and adequate breathing. Skin closure was performed with an Ethilon 5/0 suture and pain medication (0.1 mg/kg buprenorphine) was injected i.p.

Mixed bone marrow chimeras. Naive WT mice were lethally irradiated (10 Gy). 4–7 h after irradiation, animals were reconstituted with a 1:1 mixture of total bone marrow cells from μMT, WT, or *Csf2*$^{-/-}$ mice (Rauch et al., 2012). A total of 4 × 10^6 cells were injected intravenously. Animals were allowed to recover for a minimum of 8 wk.

Pneumonia models. Animals were infected i.n. or i.t. with 20 μg LPS; 2.5, 5, 7.5, or 15 × 10^6 CFU *E. coli* (American Type Culture Collection); or 2.5 × 10^4 *S. pneumoniae* (American Type Culture Collection) in a volume of 50 μl saline.

Survival. Animals injected i.t. with high doses of bacteria were monitored for survival over the course of 10 d.

Clinical score. The clinical score of each animal was assessed blinded as follows (points in parentheses). [a] appearance: normal (0), lack of grooming (1), piloerection (2), hunched up (3), above and eyes half closed (4); [b] behavior - unprovoked: normal (0), minor changes (1), less mobile and isolated (2), restless or very still (3); behavior - provoked: responsive and alert (0), unresponsive and not alert (3); [c] clinical signs: normal respiratory rate (0), slight changes (1), decreased rate with abdominal breathing (2), marked abdominal breathing and cyanosis (3); [d] hydration status: normal (0), dehydrated (5). The higher the score is, the worse the clinical situation of the animal.

Temperature. The body temperature of each animal was measured by rectal insertion of a temperature sensor while the mouse was under anesthesia.

CD116 (GM-CSF-Ra) antibody injection. 200 μg anti–GM-CSF-Rα (anti-CD116; R&D Systems) was i.pls. injected 2 h before infection with *E. coli.*

Polyclonal IgM injection. 25 μg in 50 μl polyclonal IgM (Rockland) was injected i.t. 3 h after *E. coli* infection.

Cell injection. Sorted cells, as defined below and in figures, were injected i.pls., i.p., and i.v. at time points defined in figures.

Bacteria

Bacterial titer. Bronchoalveolar lavage (BAL) samples were diluted, plated on tryptic soy agar (BD), and incubated at 37°C. The number of bacterial colonies was assessed 12–14 h later.

Detection of bacterial IgM coating after Pkh26 labeling. *E. coli* were labeled with Pkh26 (Sigma-Aldrich) according to the manufacturer's instructions. After i.t. infection with 5 × 10^6 CFU labeled *E. coli*, bacteria in the BAL were stained with anti–IgM-APC and anti–CD45.2–Pacific blue. For FACS analysis, the flow cytometric FSC and SSC setting was set to detect bacteria.

Phagocytosis assay. Phagocytosis was assessed using a pHrodo *E. coli* BioParticles Phagocytosis kit (Invitrogen) as instructed by the manufacturer.

Polyclonality assay. High protein binding capacity microtiter plate wells (Nunc Maxisorp; Sigma-Aldrich) were coated overnight at 4°C with 10^7 CFU of *S. aureus* or *P. aeruginosa*. After washing, a 1% BSA blocking solution was added to each well for 4 h at room temperature. Wells were washed and 200 μl BAL obtained 6 h after challenging WT mice with either PBS or LPS (*E. Coli* O55:B5; Sigma-Aldrich) was added to each well for 4 h at room temperature. After washing, 200 μl polyclonal anti–IgM–Alexa Fluor 488 antibodies (Abcam) diluted to 1:200 were added for 1 h at room temperature in the dark. Fluorescence was read on a Spectramax M3 plate reader (Molecular Devices). Mouse polyclonal IgM (Rockland) diluted to 1:1,000 served as a positive control for IgM.

Murine leukocytes

Isolation. Peripheral blood for flow cytometry was collected by aortic puncture, using a 50 mM EDTA solution as anticoagulant. Erythrocytes were lysed using RBC Lysis Buffer (BioLegend). Total white blood cell count was obtained by preparing a 1:10 dilution of (undiluted) peripheral blood from the orbital sinus using heparin-coated capillary tubes in RBC Lysis Buffer (BioLegend). After organ harvest, single cell suspensions were obtained as follows: for bone marrow, the femur and tibia of one leg were flushed with PBS through a 40-μm nylon mesh. Spleens and lymph nodes were homogenized through a 40-μm nylon mesh, after which erythrocyte lysis was performed using RBC Lysis Buffer (BioLegend). Lungs and liver were cut into small pieces and subjected to enzymatic digestion with 450 U/ml collagenase I, 125 U/ml collagenase XI, 60 U/ml DNase I, and 60 U/ml hyaluronidase (Sigma-Aldrich) for 1 h at 37°C while shaking. Total viable cell numbers were obtained using Trypan Blue (Cellgro; Corning). For selected experiments, the pleural space was lavaged with 2 × 1 ml PBS and the peritoneal space was lavaged with 2 × 5 ml of PBS to retrieve leukocytes. BAL was performed by flushing the lungs with 4 × 1 ml PBS to retrieve the infiltrated and resident leukocytes. Single-cell suspensions were prepared or cells were MACS-sorted according to the manufacturer's instructions and as described below.

In vitro culture. Cells were cultured in 96-well round-bottom plates (Corning) and kept in a humidified CO_2 incubator at 37°C for 24 h. B1a cells were cultured in RPMI-1640 supplemented with 10% fetal bovine

serum, 25 mM Hepes, 2 mM L-glutamine, 100 U/ml penicillin, 100 U/ml streptomycin, and 50 µM β-mercaptoethanol. All cell types were seeded at a density of 30,000 cells/100 µl medium. Where indicated, LPS was added at 10 µg/ml. Stimulation of the cells was performed by adding 0.2 µg/ml rGM-CSF in PBS. The Stat5 inhibitor (CAS 285986–31-4; Santa Cruz Biotechnology, Inc.) was used at 50 µg/ml (i.e., 200 nM).

Human leukocytes

Isolation. As part of a collaboration with the Feinstein Institute, cells were separately obtained from fresh peripheral blood samples of human adult healthy donors according to IRB-approved protocols (North Shore-LIJ Health System), and from fresh umbilical cord blood of anonymous donors provided by the Tissue Donation Program at the Feinstein Institute for Medical Research. Mononuclear cells from both adult peripheral (PBL) and umbilical cord (CB) blood were obtained by density gradient separation using lymphocyte separation medium (Cellgro). Cells were also obtained from fresh fluid of patients undergoing paracentesis or thoracentesis at Massachusetts General Hospital who required the procedure for diverse conditions, most frequently cancer. The samples were de-identified for the purposes of this study. The centesis involved sterile prepping of the skin and subcutaneous anesthesia of tissue with Lidocaine. A small 7 Fr thoracentesis catheter was placed in the fluid containing space, allowing removal of the fluid.

In vitro culture. Mononuclear cells (10^5/200 µl) were plated in medium alone (RPMI, 10% fetal calf serum, 2 mM L-glutamine, 10 mM Hepes, 100 U/ml penicillin, 100 µg/ml streptomycin, 1 mM sodium pyruvate, and 1× non-essential amino acids [Life Technologies]), or in medium with 2.5 µg/ml goat anti–human IgA + IgG + IgM (Jackson ImmunoResearch Laboratories, Inc.) and 10 ng/ml IL-2 (PeproTech) in 96-well U-bottom plates. Blocking antibodies were added at 10 µg/ml and STAT5 inhibitor at 50 µg/ml. Cells were cultured at 37°C, 5% CO_2 for 2 d. 3 h before harvesting, 0.2 µl GolgiPlug (BD) was added to the cultured cells to inhibit intracellular protein transportation. Cultured cells were then harvested and immunofluorescently stained for flow cytometric analysis (see below).

Flow cytometry

The following antibodies were used for flow cytometric analyses. Mouse: anti–CD43-FITC, S7 (BD); anti–Ly6C-FITC, AL-21 (BD); anti–IgM-FITC, II/41 (BD); anti–CD3e-FITC, 145-2C11 (BD); anti–B220-PE, RA3-6B2 (BD); anti–CD19-PE, 1D3 (BD); anti–NK1.1-PE, PK136 (BD); anti–CD49b-PE, DX5 (BD); anti–90.2-PE, 53–2.1 (BD); anti–Ly6G-PE, 1A8 (BD); anti–Ter119-PE, TER-119 (BD); anti–CD43-PE, S7 (BD); anti–GM-CSF-PE, MP1-22E9 (BD); anti–CD131-PE, JORO50 (BD); anti–IgG2A-PE, RTK2758 (BD); anti–IgG1-PE, A85-1 (BD), anti–IgM-PerCPCy5.5, R6-60.2 (BD); anti–MHCII-PerCPCy5.5, AF6-120.1 (BioLegend); anti–CD11c-PerCPCy5.5, HL3 (BD); anti–CD8-PerCPCy5.5, 53–6.7 (BD); anti–IgG2A-PerCP, RTK2758 (BD); anti–CD5-PECy7, 53–7.3 (eBioscience); anti–CD90.2-PECy7, 53–2.1 (BD); anti–CD45.1-PECy7, A20 (BD); anti–F4/80-PECy7, BM8 (BioLegend); anti–IgM-APC, II/41 (BD); anti–CD43-APC, S7 (BD); anti–BrdU-APC (BD); anti–Ly6C-APC, AL-21 (BD); anti–CD25-APC, PC61 (BD); anti–CD138-biotin, 281–2 (BD); anti–MHCII–Alexa Fluor 700, M5/114.15.2 (eBioscience); anti–CD4-Alexa Fluor 700, GK1.5 (eBioscience); anti–CD19-APCCy7, 6D5 (BioLegend); anti–CD11b-APCCy7, M1/70 (BD); anti–IgM-APCCy7, RMM-1 (BioLegend); anti–CD45.2–Pacific blue (BD); anti–CD19-Brilliant Violet 421, 6D5 (BioLegend); anti–IgM-Brilliant Violet 421, RMM-1 (BioLegend); anti–CD11b-Brilliant Violet 421, M1/70 (BioLegend); and anti-CD93, AA4.1-FITC (BD). Streptavidin–Alexa Fluor 700 (Invitrogen) was used to label biotinylated antibodies. B cell populations were identified as described previously (Rauch et al., 2012). Human: anti–CD19-APC-A700, J3-119 (Beckman Coulter); anti–GM-CSF-PE, BVD2-21C11 (BD); anti–CD20-PE-Cy7, L27 (BD); anti–IgM-PacBlue, G20-127 (BD); anti–GM-CSF (blocking), 3209 (R&D Systems); anti–GM-CSFRα (blocking; CD116), K2B7.17A (Millipore); Aqua Live/Dead Stain (Life Technologies), rat IgG2a-isotype-PE (BD).

Intracytoplasmatic staining of IgM. Isolated cells were stained for 30 min with a primary IgM antibody (i.e., APC channel) in a high concentration (1:200) to ensure saturation of surface IgM together with additional surface antibodies in normal concentration (1:700). After cell membrane permeabilization using the Cytofix/Cytoperm Plus kit (BD), intracytoplasmatic IgM was performed using the secondary IgM antibody (i.e., PerCP channel) in a lower concentration (1:350). Data were acquired on either LSRII (BD) or Gallios (Beckman Coulter) flow cytometers and analyzed with FlowJo (v8.8.6/v9.7.2; Tree Star). Cells were sorted on a FACSAria II (BD) cell sorter.

Histology and imaging

Preparation. The lungs were filled with a mixture of O.C.T. compound (Sakura) and PBS (1:1) through trachea before harvesting and embedding in a 2-methylbutane bath (Sigma-Aldrich) on dry ice. Serial 6-µm fresh-frozen sections were prepared and stored at −80°C until immunohistochemical staining was performed. Lungs from WT/µMT, GM/WT, and GM/µMT mice were stained with hematoxylin and eosin for overall histological analysis.

Immunohistochemistry. Frozen lung sections were briefly treated with 0.3% hydrogen peroxidase solution for endogenous peroxidase inactivation. The sections were incubated with a neutrophil antibody (NIMP-R14; Santa Cruz Biotechnology, Inc.) for 1 h at room temperature, followed by a biotinylated secondary antibody (Vector Laboratories) and an avidin-biotin complex (ABC) kit (Vector Laboratories). AEC (3-amino-9-ethylcarbazole) substrate (Dako), which forms a red end-product, was used for the color development. All sections were counterstained with Harris hematoxylin solution (Sigma-Aldrich) and coverslipped using an aqueous mounting medium. All the histological images were captured using a digital slide scanner (NanoZoomer 2.0RS; Hamamatsu).

Immunofluorescence microscopy. The lung sections were incubated with anti-CD19, 1D3 (BD), overnight at 4°C and Alexa Fluor 594 goat anti–rat IgG (Invitrogen), followed by anti–IgM-FITC, II/41 (BD). The slides were coverslipped using a mounting medium with DAPI (Vector Laboratories) to identify the nuclei. Images were captured and processed using an epifluorescence microscope (Eclipse 80i; Nikon Instruments Inc.).

Computed tomography (CT). Mice were imaged with CT using an Inveon small animal scanner (Siemens). CT images were reconstructed from 360 cone-beam x-ray projections with a power of 80 keV and 500 µA. The isotropic resolution of the CT images was 60 µm. Before CT acquisition, iodine contrast was infused into the pleural space. The CT acquisition time was ∼10 min. Reconstruction of datasets was done using IRW software (Siemens). Three-dimensional visualizations were produced using the DICOM viewer OsiriX (The OsiriX foundation).

Molecular Biology

ELISA. Human and mouse IgM was measured with an ELISA kit according to the manufacturer's instructions (Bethyl Laboratories, Inc.).

Luminex. Cytokines and chemokines in the bronchoalveolar lavage, the pleural space lavage, and serum were measured using a Luminex panel from Invitrogen.

ELISPOT. Cells were seeded at a density of 1,000–5,000 cells/100 µl medium. The assay (Mabtech) was performed according to the manufacturer's instructions.

RT-PCR. Total RNA was isolated from 3–10 × 10^4 FACS-sorted cells using the RNeasy Micro kit (QIAGEN) according to the manufacturer's instructions. cDNA was generated using the iScript Select cDNA Synthesis kit (Bio-Rad Laboratories). Real-time PCR was performed in duplicates using the TaqMan Gene Expression Assay System on a 7300 Real-Time PCR System (Applied Biosystems). Primers for GM-CSF (*Csf2*; *Mm01290062_m1*), Blimp1 (*Prdm1*; *Mm00476128_m1*), and housekeeping gene β-actin

(4352341E) were used (Applied Biosystems). Relative gene expression levels were calculated with the $2^{\Delta ct}$ method.

Statistics

Results were expressed as mean ± SD. Statistical tests included unpaired, two-tailed Student's *t* test using Welch's correction for unequal variances and one-way ANOVA, followed by Tukey's or Newman-Keuls Multiple Comparison Test. P-values of 0.05 or less were considered to denote significance.

The authors thank R. Gorbatov and J. Truelove for technical assistance; M. Pectasides for assistance with human cell collection; M. Greene for secretarial assistance; C. Vanderburg for help with Luminex analysis; and M. Waring and A. Chicoine for sorting cells.

This work was supported by National Institutes of Health grant R01HL095612 and R56AI104695 (to F.K. Swirski) and AI029690 (to T.L. Rothstein). G.F. Weber and I. Hilgendorf were supported by the German Research Foundation. B.G. Chousterman was supported by Société Française d'Anesthésie-Réanimation, Institut Servier, Fondation Groupe Pasteur Mutualité, and a Fulbright Scholarship (Monahan Foundation and Harvard French Scholarship Fund). C.S. Robbins was supported by the MGH Executive Committee on Research (ECOR) Postdoctoral Award. I. Theurl was supported by the Max Kade Foundation. L.M.S. Gerhardt was supported by the Boehringer Ingelheim Fonds.

The authors declare no competing financial interests.

Submitted: 12 July 2013
Accepted: 4 April 2014

REFERENCES

Ansel, K.M., R.B. Harris, and J.G. Cyster. 2002. CXCL13 is required for B1 cell homing, natural antibody production, and body cavity immunity. *Immunity*. 16:67–76. http://dx.doi.org/10.1016/S1074-7613(01)00257-6

Baumgarth, N. 2011. The double life of a B-1 cell: self-reactivity selects for protective effector functions. *Nat. Rev. Immunol.* 11:34–46. http://dx.doi.org/10.1038/nri2901

Baumgarth, N., O.C. Herman, G.C. Jager, L.E. Brown, L.A. Herzenberg, and J. Chen. 2000. B-1 and B-2 cell–derived immunoglobulin M antibodies are nonredundant components of the protective response to influenza virus infection. *J. Exp. Med.* 192:271–280. http://dx.doi.org/10.1084/jem.192.2.271

Bezbradica, J.S., L.E. Gordy, A.K. Stanic, S. Dragovic, T. Hill, J. Hawiger, D. Unutmaz, L. Van Kaer, and S. Joyce. 2006. Granulocyte-macrophage colony-stimulating factor regulates effector differentiation of invariant natural killer T cells during thymic ontogeny. *Immunity*. 25:487–497. http://dx.doi.org/10.1016/j.immuni.2006.06.017

Bo, L., F. Wang, J. Zhu, J. Li, and X. Deng. 2011. Granulocyte-colony stimulating factor (G-CSF) and granulocyte-macrophage colony stimulating factor (GM-CSF) for sepsis: a meta-analysis. *Crit. Care*. 15:R58. http://dx.doi.org/10.1186/cc10031

Boes, M., A.P. Prodeus, T. Schmidt, M.C. Carroll, and J. Chen. 1998. A critical role of natural immunoglobulin M in immediate defense against systemic bacterial infection. *J. Exp. Med.* 188:2381–2386. http://dx.doi.org/10.1084/jem.188.12.2381

Bradley, T.R., and D. Metcalf. 1966. The growth of mouse bone marrow cells in vitro. *Aust. J. Exp. Biol. Med. Sci.* 44:287–300. http://dx.doi.org/10.1038/icb.1966.28

Carey, B., and B.C. Trapnell. 2010. The molecular basis of pulmonary alveolar proteinosis. *Clin. Immunol.* 135:223–235. http://dx.doi.org/10.1016/j.clim.2010.02.017

Cerutti, A., M. Cols, and I. Puga. 2013. Marginal zone B cells: virtues of innate-like antibody-producing lymphocytes. *Nat. Rev. Immunol.* 13:118–132. http://dx.doi.org/10.1038/nri3383

Choi, Y.S., and N. Baumgarth. 2008. Dual role for B-1a cells in immunity to influenza virus infection. *J. Exp. Med.* 205:3053–3064. http://dx.doi.org/10.1084/jem.20080979

Dranoff, G., A.D. Crawford, M. Sadelain, B. Ream, A. Rashid, R.T. Bronson, G.R. Dickersin, C.J. Bachurski, E.L. Mark, J.A. Whitsett, et al. 1994. Involvement of granulocyte-macrophage colony-stimulating factor in pulmonary homeostasis. *Science*. 264:713–716. http://dx.doi.org/10.1126/science.8171324

Düber, S., M. Hafner, M. Krey, S. Lienenklaus, B. Roy, E. Hobeika, M. Reth, T. Buch, A. Waisman, K. Kretschmer, and S. Weiss. 2009. Induction of B-cell development in adult mice reveals the ability of bone marrow to produce B-1a cells. *Blood*. 114:4960–4967. http://dx.doi.org/10.1182/blood-2009-04-218156

Ehrenstein, M.R., and C.A. Notley. 2010. The importance of natural IgM: scavenger, protector and regulator. *Nat. Rev. Immunol.* 10:778–786. http://dx.doi.org/10.1038/nri2849

Esperatti, M., M. Ferrer, A. Theessen, A. Liapikou, M. Valencia, L.M. Saucedo, E. Zavala, T. Welte, and A. Torres. 2010. Nosocomial pneumonia in the intensive care unit acquired by mechanically ventilated versus nonventilated patients. *Am. J. Respir. Crit. Care Med.* 182:1533–1539. http://dx.doi.org/10.1164/rccm.201001-0094OC

Esplin, B.L., R.S. Welner, Q. Zhang, L.A. Borghesi, and P.W. Kincade. 2009. A differentiation pathway for B1 cells in adult bone marrow. *Proc. Natl. Acad. Sci. USA*. 106:5773–5778. http://dx.doi.org/10.1073/pnas.0811632106

Fabrizio, K., A. Groner, M. Boes, and L.A. Pirofski. 2007. A human monoclonal immunoglobulin M reduces bacteremia and inflammation in a mouse model of systemic pneumococcal infection. *Clin. Vaccine Immunol.* 14:382–390. http://dx.doi.org/10.1128/CVI.00374-06

Fairfax, K.A., L.M. Corcoran, C. Pridans, N.D. Huntington, A. Kallies, S.L. Nutt, and D.M. Tarlinton. 2007. Different kinetics of blimp-1 induction in B cell subsets revealed by reporter gene. *J. Immunol.* 178:4104–4111. http://dx.doi.org/10.4049/jimmunol.178.7.4104

Greter, M., J. Helft, A. Chow, D. Hashimoto, A. Mortha, J. Agudo-Cantero, M. Bogunovic, E.L. Gautier, J. Miller, M. Leboeuf, et al. 2012. GM-CSF controls nonlymphoid tissue dendritic cell homeostasis but is dispensable for the differentiation of inflammatory dendritic cells. *Immunity*. 36:1031–1046. http://dx.doi.org/10.1016/j.immuni.2012.03.027

Guthridge, M.A., J.A. Powell, E.F. Barry, F.C. Stomski, B.J. McClure, H. Ramshaw, F.A. Felquer, M. Dottore, D.T. Thomas, B. To, et al. 2006. Growth factor pleiotropy is controlled by a receptor Tyr/Ser motif that acts as a binary switch. *EMBO J.* 25:479–489. http://dx.doi.org/10.1038/sj.emboj.7600948

Ha, S.A., M. Tsuji, K. Suzuki, B. Meek, N. Yasuda, T. Kaisho, and S. Fagarasan. 2006. Regulation of B1 cell migration by signals through Toll-like receptors. *J. Exp. Med.* 203:2541–2550. http://dx.doi.org/10.1084/jem.20061041

Hamilton, J.A. 2008. Colony-stimulating factors in inflammation and autoimmunity. *Nat. Rev. Immunol.* 8:533–544. http://dx.doi.org/10.1038/nri2356

Hamilton, J.A., and A. Achuthan. 2013. Colony stimulating factors and myeloid cell biology in health and disease. *Trends Immunol.* 34:81–89. http://dx.doi.org/10.1016/j.it.2012.08.006

Hege, K.M., K. Jooss, and D. Pardoll. 2006. GM-CSF gene-modifed cancer cell immunotherapies: of mice and men. *Int. Rev. Immunol.* 25:321–352. http://dx.doi.org/10.1080/08830180600992498

Holodick, N.E., K. Repetny, X. Zhong, and T.L. Rothstein. 2009. Adult BM generates $CD5^+$ B1 cells containing abundant N-region additions. *Eur. J. Immunol.* 39:2383–2394. http://dx.doi.org/10.1002/eji.200838920

Huffman, J.A., W.M. Hull, G. Dranoff, R.C. Mulligan, and J.A. Whitsett. 1996. Pulmonary epithelial cell expression of GM-CSF corrects the alveolar proteinosis in GM-CSF-deficient mice. *J. Clin. Invest.* 97:649–655. http://dx.doi.org/10.1172/JCI118461

Jones, R.N. 2010. Microbial etiologies of hospital-acquired bacterial pneumonia and ventilator-associated bacterial pneumonia. *Clin. Infect. Dis.* 51:S81–S87. http://dx.doi.org/10.1086/653053

Jonjić, N., G. Peri, S. Bernasconi, F.L. Sciacca, F. Colotta, P. Pelicci, L. Lanfrancone, and A. Mantovani. 1992. Expression of adhesion molecules and chemotactic cytokines in cultured human mesothelial cells. *J. Exp. Med.* 176:1165–1174. http://dx.doi.org/10.1084/jem.176.4.1165

Kawahara, T., H. Ohdan, G. Zhao, Y.G. Yang, and M. Sykes. 2003. Peritoneal cavity B cells are precursors of splenic IgM natural antibody-producing cells. *J. Immunol.* 171:5406–5414. http://dx.doi.org/10.4049/jimmunol.171.10.5406

Kimura, A., M.A. Rieger, J.M. Simone, W. Chen, M.C. Wickre, B.M. Zhu, P.S. Hoppe, J.J. O'Shea, T. Schroeder, and L. Hennighausen. 2009. The transcription factors STAT5A/B regulate GM-CSF–mediated granulopoiesis. *Blood*. 114:4721–4728. http://dx.doi.org/10.1182/blood-2009-04-216390

Klevens, R.M., J.R. Edwards, C.L.J. Richards Jr., T.C. Horan, R.P. Gaynes, D.A. Pollock, and D.M. Cardo. 2007. Estimating health care-associated infections and deaths in U.S. hospitals, 2002. *Public Health Rep*. 122:160–166.

LaRosa, S.P., and S.M. Opal. 2012. Immune aspects of sepsis and hope for new therapeutics. *Curr. Infect. Dis. Rep*. 14:474–483. http://dx.doi.org/10.1007/s11908-012-0276-2

Le, D.T., D.M. Pardoll, and E.M. Jaffee. 2010. Cellular vaccine approaches. *Cancer J.* 16:304–310. http://dx.doi.org/10.1097/PPO.0b013e3181eb33d7

Litvack, M.L., M. Post, and N. Palaniyar. 2011. IgM promotes the clearance of small particles and apoptotic microparticles by macrophages. *PLoS ONE*. 6:e17223. http://dx.doi.org/10.1371/journal.pone.0017223

Magret, M., T. Lisboa, I. Martin-Loeches, R. Máñez, M. Nauwynck, H. Wrigge, S. Cardellino, E. Díaz, D. Koulenti, and J. Rello; EU-VAP/CAP Study Group. 2011. Bacteremia is an independent risk factor for mortality in nosocomial pneumonia: a prospective and observational multicenter study. *Crit. Care*. 15:R62. http://dx.doi.org/10.1186/cc10036

Medzhitov, R. 2007. Recognition of microorganisms and activation of the immune response. *Nature*. 449:819–826. http://dx.doi.org/10.1038/nature06246

Metcalf, D., N.A. Nicola, S. Mifsud, and L. Di Rago. 1999. Receptor clearance obscures the magnitude of granulocyte-macrophage colony-stimulating factor responses in mice to endotoxin or local infections. *Blood*. 93:1579–1585.

Mizgerd, J.P. 2008. Acute lower respiratory tract infection. *N. Engl. J. Med*. 358:716–727. http://dx.doi.org/10.1056/NEJMra074111

Moon, H., J.G. Lee, S.H. Shin, and T.J. Kim. 2012. LPS-induced migration of peritoneal B-1 cells is associated with upregulation of CXCR4 and increased migratory sensitivity to CXCL12. *J. Korean Med. Sci*. 27:27–35. http://dx.doi.org/10.3346/jkms.2012.27.1.27

Mui, A.L., H. Wakao, A.M. O'Farrell, N. Harada, and A. Miyajima. 1995. Interleukin-3, granulocyte-macrophage colony stimulating factor and interleukin-5 transduce signals through two STAT5 homologs. *EMBO J.* 14:1166–1175.

Nurieva, R.I., A. Podd, Y. Chen, A.M. Alekseev, M. Yu, X. Qi, H. Huang, R. Wen, J. Wang, H.S. Li, et al. 2012. STAT5 protein negatively regulates T follicular helper (Tfh) cell generation and function. *J. Biol. Chem*. 287:11234–11239. http://dx.doi.org/10.1074/jbc.M111.324046

Nutt, S.L., K.A. Fairfax, and A. Kallies. 2007. BLIMP1 guides the fate of effector B and T cells. *Nat. Rev. Immunol*. 7:923–927. http://dx.doi.org/10.1038/nri2204

Racine, R., and G.M. Winslow. 2009. IgM in microbial infections: taken for granted? *Immunol. Lett*. 125:79–85. http://dx.doi.org/10.1016/j.imlet.2009.06.003

Rauch, P.J., A. Chudnovskiy, C.S. Robbins, G.F. Weber, M. Etzrodt, I. Hilgendorf, E. Tiglao, J.L. Figueiredo, Y. Iwamoto, I. Theurl, et al. 2012. Innate response activator B cells protect against microbial sepsis. *Science*. 335:597–601. http://dx.doi.org/10.1126/science.1215173

Savitsky, D., and K. Calame. 2006. B-1 B lymphocytes require Blimp-1 for immunoglobulin secretion. *J. Exp. Med*. 203:2305–2314. http://dx.doi.org/10.1084/jem.20060411

Schwartz, J.T., J.H. Barker, M.E. Long, J. Kaufman, J. McCracken, and L.A. Allen. 2012. Natural IgM mediates complement-dependent uptake of Francisella tularensis by human neutrophils via complement receptors 1 and 3 in nonimmune serum. *J. Immunol*. 189:3064–3077. http://dx.doi.org/10.4049/jimmunol.1200816

Scott, J.A., W.A. Brooks, J.S. Peiris, D. Holtzman, and E.K. Mulholland. 2008. Pneumonia research to reduce childhood mortality in the developing world. *J. Clin. Invest*. 118:1291–1300. http://dx.doi.org/10.1172/JCI33947

Shapiro-Shelef, M., K.I. Lin, L.J. McHeyzer-Williams, J. Liao, M.G. McHeyzer-Williams, and K. Calame. 2003. Blimp-1 is required for the formation of immunoglobulin secreting plasma cells and pre-plasma memory B cells. *Immunity*. 19:607–620. http://dx.doi.org/10.1016/S1074-7613(03)00267-X

Snapper, C.M., M.A. Moorman, F.R. Rosas, M.R. Kehry, C.R. Maliszewski, and J.J. Mond. 1995. IL-3 and granulocyte-macrophage colony-stimulating factor strongly induce Ig secretion by sort-purified murine B cell activated through the membrane Ig, but not the CD40, signaling pathway. *J. Immunol*. 154:5842–5850.

Stämpfli, M.R., R.E. Wiley, G.S. Neigh, B.U. Gajewska, X.F. Lei, D.P. Snider, Z. Xing, and M. Jordana. 1998. GM-CSF transgene expression in the airway allows aerosolized ovalbumin to induce allergic sensitization in mice. *J. Clin. Invest*. 102:1704–1714. http://dx.doi.org/10.1172/JCI4160

Stanley, E., G.J. Lieschke, D. Grail, D. Metcalf, G. Hodgson, J.A. Gall, D.W. Maher, J. Cebon, V. Sinickas, and A.R. Dunn. 1994. Granulocyte/macrophage colony-stimulating factor-deficient mice show no major perturbation of hematopoiesis but develop a characteristic pulmonary pathology. *Proc. Natl. Acad. Sci. USA*. 91:5592–5596. http://dx.doi.org/10.1073/pnas.91.12.5592

Timmerman, J.M., J.M. Vose, D.K. Czerwinski, W.K. Weng, D. Ingolia, M. Mayo, D.W. Denney, and R. Levy. 2009. Tumor-specific recombinant idiotype immunisation after chemotherapy as initial treatment for follicular non-Hodgkin lymphoma. *Leuk. Lymphoma*. 50:37–46. http://dx.doi.org/10.1080/10428190802563355

Venkatachalam, V., J.O. Hendley, and D.F. Willson. 2011. The diagnostic dilemma of ventilator-associated pneumonia in critically ill children. *Pediatr. Crit. Care Med*. 12:286–296. http://dx.doi.org/10.1097/PCC.0b013e3181fe2ffb

Williams, B.G., E. Gouws, C. Boschi-Pinto, J. Bryce, and C. Dye. 2002. Estimates of world-wide distribution of child deaths from acute respiratory infections. *Lancet Infect. Dis*. 2:25–32. http://dx.doi.org/10.1016/S1473-3099(01)00170-0

Yang, Y., J.W. Tung, E.E. Ghosn, L.A. Herzenberg, and L.A. Herzenberg. 2007. Division and differentiation of natural antibody-producing cells in mouse spleen. *Proc. Natl. Acad. Sci. USA*. 104:4542–4546. http://dx.doi.org/10.1073/pnas.0700001104

Zhan, Y., G.J. Lieschke, D. Grail, A.R. Dunn, and C. Cheers. 1998. Essential roles for granulocyte-macrophage colony-stimulating factor (GM-CSF) and G-CSF in the sustained hematopoietic response of Listeria monocytogenes-infected mice. *Blood*. 91:863–869.